

Time Lags between the 22 and 37 GHz Bursts of 48 Radio-loud AGNs *

Wen-Guo Deng^{1,2}, Jin-Ming Bai¹, Li Zhang² and Xian Yang^{1,2}

¹ National Astronomical Observatories/Yunnan Observatory, Chinese Academy of Sciences, Kunming 650011; dwg906@ynao.ac.cn

² Physics Department, Yunnan University, Kunming 650091

Received 2007 May 4; accepted 2007 July 6

Abstract Based on the light curves at 22 and 37 GHz from the Metsahovi monitoring program, we investigate the time lags between the two radio bands for 48 radio-loud AGNs. DCF and ZDCF analyses are applied to the data. Our results show that there is a strong correlation between the two radio frequencies for all the sources, with the variations in the light curves at 37 GHz leading the ones at 22 GHz in general. There is no obvious differences between different sub-class AGNs as regards the time lag. In two sources, it was found that the bursts at the lower frequency lead the ones at the higher frequency. One possible explanation is that electron acceleration dominates the light curve until the radiation reaches the maximum. Some sources, such as 3C 273, 3C 279, 3C 345 and 3C 454.3, have good enough data, so we can calculate their lags burst-by-burst. Our calculations show that different outbursts have different lags. Some bursts have positive lags, most of bursts have no clear lags, and a few have negative lags. This result means that different bursts are triggered by different mechanisms, and the interpretation for the result involves both an intrinsic and a geometric mechanism. The positive lags are well consistent with the shock model, and we use these lags to calculate the typical magnetic field strength of the radiating region.

Key words: galaxies: active — galaxies: individual (3C 273, 3C 279, 3C 345, 3C 454.3) — methods: data analysis

1 INTRODUCTION

Radio-loud Active Galactic Nuclei (AGNs) display variability over a wide range of wavebands (Xie et al. 1994). It is generally accepted that outbursts in these AGNs are triggered by growing shocks in jets that are shot out from the center of the galaxy (Marscher & Gear 1985; Valtaoja et al. 1992; Türler et al. 2000; Yi & Xie 2008). The generalized shock model (Valtaoja et al. 1992; Lainela 1994) explains how a shock grows and decays, and how the outburst looks at different frequencies. The model predicts the time lags between the outbursts at different frequencies. So far, light curves are an efficient tool to investigate the origins of shocks in jets.

Correlation between flares or bursts at different frequencies in AGNs has been investigated since the beginning of the 1970's. Some objects have been studied individually in the literature, e.g. 3C 120 (Usher 1972), BL Lac (Andrew et al. 1974; Tornikoski et al. 1994a), PKS 0420–01 (Dent et al. 1979), 3C 446 (Bregman et al. 1988), OJ 287 (Kikuchi et al. 1973; Kinman et al. 1974; Usher 1979; Valtaoja et al. 1987), 3C 454.3 (Villata et al. 2007), and AO 0235+164 (Balonek & Dent 1980; Roy et al. 2000; Raiteri et al. 2001). It is clear that there is some correlation between the variations at different frequencies at least in

* Supported by the National Natural Science Foundation of China.

some sources, e.g. 3C 279, 3C 345 (Tornikoski et al. 1994b), AO 0235+164 (Clements et al. 1995; Raiteri et al. 2001), and GC 0109+224 (Ciprini et al. 2004).

The first studies on several sources at a time were carried out by Usher (1975) and Pomphrey et al. (1976). Usher (1975) studied the correlation between the radio spectral index and optical variability. Pomphrey et al. (1976) studied the optical and radio light curves, and found a strong correlation in only one object, OJ 287. A search for correlations in a large sample of 45 AGNs was done by Balonek (1982), who found that 11 sources exhibited a probable correlation between the optical and radio flares (or bursts) with time lags up to several hundred days, while correlation was not found in 15 sources. Other extensive studies were done by Tornikoski et al. (1994b), Clements et al. (1995), and Hanski et al. (2002).

Recently, Pyatunina et al. (2006) examined the four gamma-ray blazars that have been nearly continuously monitored at University of Michigan Radio Astronomy Observatory and Metsähovi Radio Observatory: 0458–020, 0528+134, 1730–130 and 2230+114, in frequency range from 4.8 to 37 GHz, and found frequency-dependent time-delays ranging from ~ 0.3 to ~ 1.0 yr.

However, the research on correlations in AGNs between different radio bands are not detailed, and the samples used in the previous works are very small. Thanks to the Metsähovi radio monitoring program, a large sample of radio light curves is now available. We have compared the 22 GHz light curves with the 37 GHz light curves for a large number of radio sources, using Discrete Correlation Function (DCF) and z -transformed discrete correlation function (ZDCF). We used ZDCF to obtain the uncertainties of the time lags. For some sources with good data sampling, we calculated the time lags burst-by-burst. The data sample selection is described in Section 2. The methods of analysis and the results are presented in Sections 3 and 4, respectively. A discussion and conclusions are presented in Section 5.

2 THE DATA AND SAMPLE SELECTION

From the Metsähovi radio monitoring list, we selected objects with light curves that are enough sampled for our analysis. Details of the Metsähovi radio monitoring program and the radio data are described in Teräsraanta et al. (1992, 1998, 2004, 2005). Our sample contains 48 AGNs, of which 35 are quasars and 10 are BL Lacs, and the rest are Seyfert galaxies (see Table 1). The objects are classified as “B” = BL Lac objects, “Q” = Quasar, “A” = Active galaxies : Seyfert 1s, Seyfert 2s and LINERs, fainter than $M_B = -23$. The quasar/BL Lac classification is adopted from Veron-Cetty & Veron (2006).

3 METHODS OF ANALYSIS

DCF was introduced by Edelson & Krolik (1988). This method is similar to the classical cross correlation function which has been widely adopted to calculate time lags (e.g. Norris et al. 2000; Peng et al. 2007; Yi et al. 2006, 2008; Zhang et al. 2007), but overcomes some of the shortcomings of the classical cross correlation method. It does not require interpolation in the data sets, and provides meaningful error estimates. Hufnagel & Bregman (1992) generalized it and used it to correlate optical light curves with radio light curves. In this paper the formula adopted by Edelson & Krolik (1988) is used. First, the set of unbinned discrete correlations (UDCF_{ij}) is calculated between each pair (a_i, b_j) in data sets a and b . UDCF_{ij} is defined as

$$\text{UDCF}_{ij} = \frac{(a_i - \bar{a})(b_j - \bar{b})}{\sqrt{(\sigma_a^2 - e_a^2)(\sigma_b^2 - e_b^2)}}, \quad (1)$$

where a_i and b_j are data points in the data sets a and b , \bar{a} , \bar{b} the mean values, σ_a and σ_b the standard deviations of the data sets, e_a and e_b the measurement error associated with the data sets a and b . For each UDCF_{ij} value the corresponding time difference $\Delta t_{ij} = t_i - t_j$ is calculated. The next step is to average those points in UDCF_{ij} that have the same time differences Δt_{ij} . The UDCF_{ij} values for which $\tau - \Delta\tau/2 \leq \Delta t_{ij} \leq \tau + \Delta\tau/2$ are binned to obtain the DCF value for the given time lag. Here τ is the time lag and $\Delta\tau$ the chosen bin size. DCF(τ) is then defined as

$$\text{DCF}(\tau) = \frac{1}{M} \sum \text{UDCF}_{ij}(\tau), \quad (2)$$

where M is the number of UDCF_{ij} s in the bin. The standard error for a bin used here is

$$\sigma_{\text{DCF}} = \frac{1}{\sqrt{(M-1)(M'-1)}} \left\{ \sum [\text{UDCF}_{ij} - \text{DCF}(\tau)]^2 \right\}^{1/2}, \quad (3)$$

Table 1 Data of 48 objects, “B” = BL Lac objects, “Q” =Quasar, “A” = Active galaxies: Seyfert 1s, Seyfert 2s.

Name	Class	RAJ2000	DEJ2000	Z	Data	DCF vr	ZDCF vr	bin vr
III Zw 2	A	00 10 31.0	+10 58 28	0.089	all	0.14	$0.21_{-0.22}^{+0.06}$	0.05
PKS 0106+01	Q	01 08 38.8	+01 35 00	2.107	all	0.02	$0.06_{-0.21}^{+0.06}$	0.10
S2 0109+22	B	01 12 05.8	+22 44 39	?	all	0.16	$0.24_{-0.24}^{+0.07}$	0.10
DA 55	Q	01 36 58.6	+47 51 29	0.859	all	0.04	$0.11_{-0.35}^{+0.08}$	0.10
PKS 0202+14	A	02 04 50.4	+15 14 11	0.405	all	0.32	$0.19_{-0.22}^{+0.07}$	0.10
B2 0234+28	Q	02 37 52.4	+28 48 10	1.207	all	0.08	$0.10_{-0.17}^{+0.06}$	0.10
					92–96	-0.29	$-0.25_{-0.01}^{+0.01}$	0.05
AO 0235+164	Q	02 38 38.9	+16 37 00	0.940	all	0.10	$0.20_{-0.31}^{+0.07}$	0.05
NRAO 140	Q	03 36 30.1	+32 18 30	1.259	all	0.25	$0.20_{-0.29}^{+0.07}$	0.10
PKS 0420–01	Q	04 23 15.8	-01 20 33	0.915	all	0.10	$0.33_{-0.33}^{+0.07}$	0.10
PKS 0422+00	B	04 24 46.8	+00 36 07	0.31	all	0.02	$0.21_{-0.22}^{+0.07}$	0.10
3C120	A	04 33 11.1	+05 21 15	0.033	all	0.07	$0.34_{-0.39}^{+0.08}$	0.02
PKS 0528+134	Q	05 30 56.5	+13 31 55	2.070	all	0.10	$0.28_{-0.32}^{+0.08}$	0.10
B2 0552+39A	Q	05 55 30.8	+39 48 49	2.363	all	0.10	$0.00_{-0.07}^{+0.01}$	0.05
OH 471	Q	06 46 32.0	+44 51 17	3.408	all	0.97	$0.04_{-0.17}^{+0.05}$	0.20
PKS 0735+17	B	07 38 07.4	+17 42 19	0.424	all	0.00	$0.20_{-0.28}^{+0.08}$	0.20
PKS 0736+01	Q	07 39 18.0	+01 37 04	0.191	all	0.05	$0.28_{-0.36}^{+0.10}$	0.05
PKS 0754+100	B	07 57 06.7	+09 56 35	0.266	all	0.05	$0.23_{-0.23}^{+0.07}$	0.05
SBS 0804+499	Q	08 08 39.6	+49 50 37	1.432	all	0.02	$-0.09_{-0.13}^{+0.04}$	0.05
OJ 425	B	08 18 16.1	+42 22 46	0.530	all	-0.41	$0.04_{-0.10}^{+0.03}$	0.20
OJ 287	B	08 54 48.8	+20 06 30	0.306	all	0.00	$0.38_{-0.45}^{+0.12}$	0.05
					91	0.00	$0.005_{-0.001}^{+0.002}$	0.02
					02	0.00	$0.001_{-0.001}^{+0.004}$	0.05
B2 0923+39	Q	09 27 03.0	+39 02 21	0.698	all	0.33	$0.19_{-0.51}^{+0.07}$	0.10
PKS 1055+01	Q	10 58 29.6	+01 33 58	0.888	all	0.00	$0.27_{-0.36}^{+0.11}$	0.20
4C 29.45	Q	11 59 31.9	+29 14 45	0.729	all	0.00	$0.29_{-0.35}^{+0.08}$	0.05
PKS 1222+21	Q	12 24 54.5	+21 22 46	0.435	all	0.09	$0.07_{-0.10}^{+0.04}$	0.10
3C 273	Q	12 29 06.7	+02 03 08	0.158	all	0.25	$0.71_{-0.71}^{+0.11}$	0.05
					86–87	0.05	$0.06_{-0.004}^{+0.007}$	0.10
					88–89	0.25	$0.22_{-0.003}^{+0.006}$	0.02
					91–92	0.05	$0.07_{-0.003}^{+0.009}$	0.02
					96–97	0.15	$0.14_{-0.001}^{+0.003}$	0.02
					97–99	0.07	$0.08_{-0.013}^{+0.005}$	0.05
					02–03	0.09	$0.08_{-0.008}^{+0.02}$	0.05
3C 279	Q	12 56 11.1	-05 47 21	0.538	all	0.38	$-0.46_{-0.56}^{+0.12}$	0.10
					88–89	0.09	$0.13_{-0.04}^{+0.03}$	0.10
					91	-0.04	$-0.03_{-0.003}^{+0.005}$	0.01
					01–02	0.05	$-0.045_{-0.015}^{+0.008}$	0.02
B2 1308+32	Q	13 10 28.7	+32 20 44	0.997	all	-0.03	$0.18_{-0.26}^{+0.07}$	0.10
PKS 1413+135	B	14 15 58.8	+13 20 24	0.247	all	0.10	$0.02_{-0.24}^{+0.06}$	0.10
OQ 530	B	14 19 46.6	+54 23 14	0.152	all	0.00	$0.01_{-0.16}^{+0.04}$	0.10
PKS 1502+106	Q	15 04 24.9	+10 29 40	1.839	all	0.15	$0.16_{-0.21}^{+0.07}$	0.10
PKS 1510–08	Q	15 12 50.5	-09 06 00	0.360	all	0.00	$0.19_{-0.19}^{+0.05}$	0.10
4C 14.60	Q	15 40 49.5	+14 47 46	0.605	all	0.37	$0.28_{-0.27}^{+0.07}$	0.10
DA 406	Q	16 13 41.1	+34 12 48	1.401	all	0.10	$-0.097_{-0.167}^{+0.042}$	0.10
B2 1633+38	Q	16 35 15.5	+38 08 03	1.807	all	0.22	$0.23_{-0.37}^{+0.07}$	0.05
OS 562	Q	16 38 13.6	+57 20 24	0.751	all	0.09	$0.02_{-0.11}^{+0.05}$	0.10
3C 345	Q	16 42 58.8	+39 48 37	0.594	all	0.39	$0.10_{-0.33}^{+0.06}$	0.10
					91–92	0.12	$0.17_{-0.01}^{+0.005}$	0.02
					95–96	0.14	$0.13_{-0.01}^{+0.004}$	0.02
MARK 501	B	16 53 52.2	+39 45 36	0.033	all	0.19	$0.65_{-0.16}^{+0.04}$	0.10

Table 1 – *Continued.*

Name	Class	RAJ2000	DEJ2000	Z	Data	$\frac{\text{DCF}}{\text{yr}}$	$\frac{\text{ZDCF}}{\text{yr}}$	$\frac{\text{bin}}{\text{yr}}$
OT 566	Q	17 40 37.0	+52 11 43	1.379	all	0.00	$0.12_{-0.11}^{+0.04}$	0.10
PKS 1741–03	Q	17 43 58.8	–03 50 05	1.057	all	0.08	$0.16_{-0.28}^{+0.07}$	0.02
OT 081	Q	17 51 32.8	+09 39 02	0.320	all	0.03	$0.09_{-0.25}^{+0.05}$	0.05
TEX 2005+403	Q	20 07 45.0	+40 29 48	1.736	all	1.06	$0.33_{-0.36}^{+0.08}$	0.20
PKS 2134+004	Q	21 36 38.7	+00 41 55	1.932	all	0.01	$0.19_{-0.30}^{+0.08}$	0.20
PKS 2145+06	Q	21 48 05.5	+06 57 39	0.999	all	0.14	$0.32_{-0.35}^{+0.06}$	0.05
					92–97	0.00	$0.02_{-0.08}^{+0.03}$	0.10
BL LAC	B	22 02 43.3	+42 16 39	0.069	all	0.00	$0.08_{-0.39}^{+0.06}$	0.05
					93	0.02	$0.01_{-0.004}^{+0.001}$	0.02
B2 2201+31A	Q	22 03 14.9	+31 45 38	0.298	all	0.08	$0.07_{-0.18}^{+0.05}$	0.10
3C 446	Q	22 25 47.2	–04 57 01	1.404	all	0.16	$0.14_{-0.21}^{+0.07}$	0.05
CTA 102	Q	22 32 36.4	+11 43 51	1.037	all	0.31	$0.05_{-0.15}^{+0.05}$	0.05
					97–98	0.13	$0.20_{-0.01}^{+0.006}$	0.04
3C 454.3	Q	22 53 57.7	+16 08 53	0.859	all	–0.04	$0.04_{-0.29}^{+0.05}$	0.02
					90–91	0.11	$0.05_{-0.005}^{+0.009}$	0.02
					94–95	0.08	$0.15_{-0.007}^{+0.015}$	0.01
					03	0.07	$0.04_{-0.006}^{+0.005}$	0.02

where M' is the number of different measurement times t_i for the time series a in the bin. When $a = b$, the autocorrelation DCF is produced. In most cases, an evident peak in the cross correlation function means a strong correlation between the two data series. The higher the peak, the stronger the correlation. A positive peak of the DCF means correlation in which the data set a leads the data set b , and conversely for a negative peak. To obtain a more reliable estimate of the time lag, a better method is to calculate the centroid of the DCF, $\tau_c = (\sum_i \tau_i \text{DCF}_i) / (\sum_i \text{DCF}_i)$, where the summations run over the points with DCF values close to the peak (Raiteri et al. 2003, 2005). Here, the centroid τ_c is computed using those points for which $\text{DCF}(\tau) \geq 0.8 \text{DCF}_{\text{peak}}$, where DCF_{peak} is the maximum value of the DCF (Peterson 2001). We also carry out analyses of the ZDCF (Alexander 1997) for those sources. In this, the data bin is taken with equal population, rather than with equal $\Delta\tau$. The z -transform's convergence requires a minimum of $n_{\text{min}} = 11$ points per bin, otherwise it cannot give a continuous correlation function for $\Delta\tau$. Nevertheless, the ZDCF method can provide us the uncertainty of the lag without interpolation. Sometimes, when the data sampling is uneven and very sparse, the result may show some spurious lags. We use these two methods to obtain more credible lags.

4 RESULTS

We apply the DCF and ZDCF to all the sources, and the result is shown in Table 1. In the DCF analysis, bin sizes of 0.01–0.2 yr are used. Several sources such as 3C 273, 3C 279, 3C 345 and 3C454.3, have a good data point distribution. We calculated the time lags of those sources burst-by-burst, and will make individual checks in the following subsections. The correlation between the two radio frequencies is strong for all the sources, with no difference between the different sub-classes. See Table 1.

4.1 3C 273

This source is a flat spectrum radio quasar (FSRQ). The 24 yr data show a 0.25 yr lag between 22 and 37 GHz in the DCF analysis. The ZDCF results show a 0.71 yr lag, but with a very large uncertainty, and this is consistent with the DCF result within the uncertainty of ZDCF. The bursts of 88–89 (see Fig. 5) and 96–97 show prominent lags with the 37 GHz variations leading the 22 GHz variations. The DCF and ZDCF results are well consistent with each other, and the uncertainties in the lags are very small. Other bursts of this source show no lags. The detailed result is in Table 1.

4.2 3C 279

The DCF of all data shows a positive lag of 0.38 yr, while the ZDCF result shows a negative peak at 0.46 yr, but the result is not reliable because it is very uncertain. Burst-by-burst analysis does not show any obvious

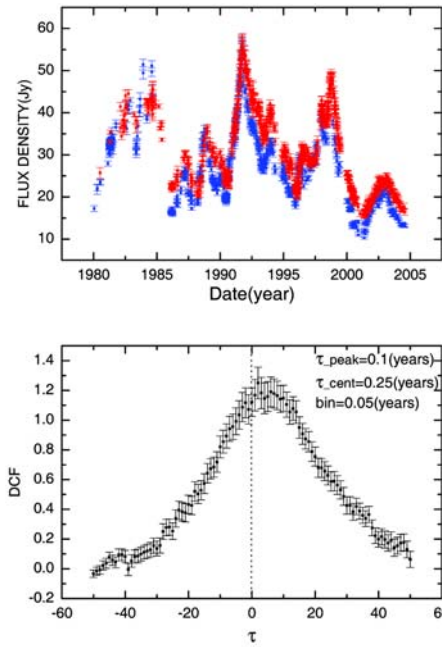


Fig. 1 Top panel shows the light curve of 3C 273 at 22 GHz (red dots) and 37 GHz (blue dots), bottom panel the calculated DCF.

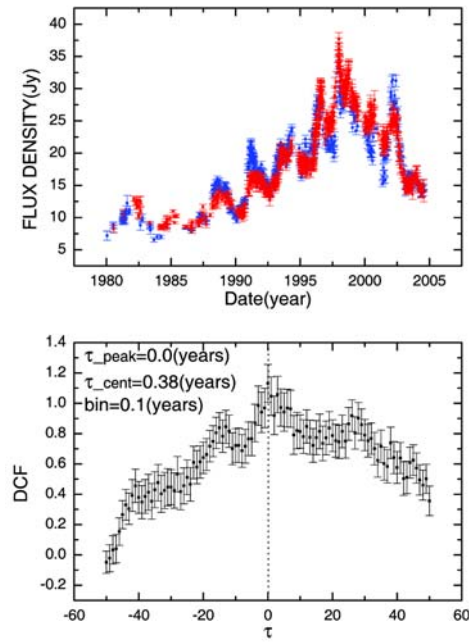


Fig. 2 Top panel shows the light curve of 3C 279 at 22 GHz (red dots) and 37 GHz (blue dots), bottom panel the DCF result.

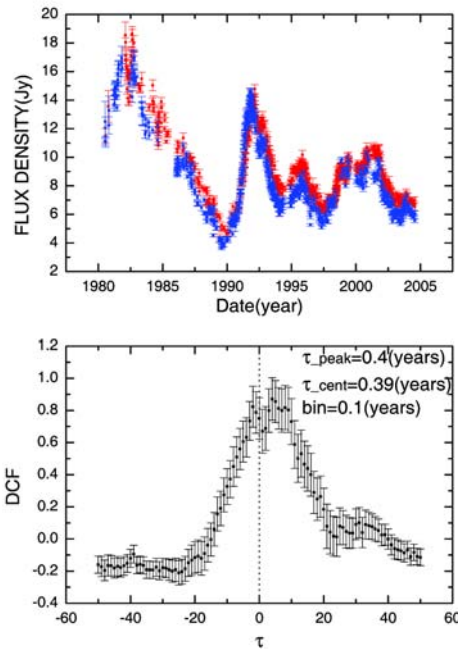


Fig. 3 Top panel shows the light curve of 3C 345 at 22 GHz (red dots) and 37 GHz (blue dots), bottom panel the DCF result.

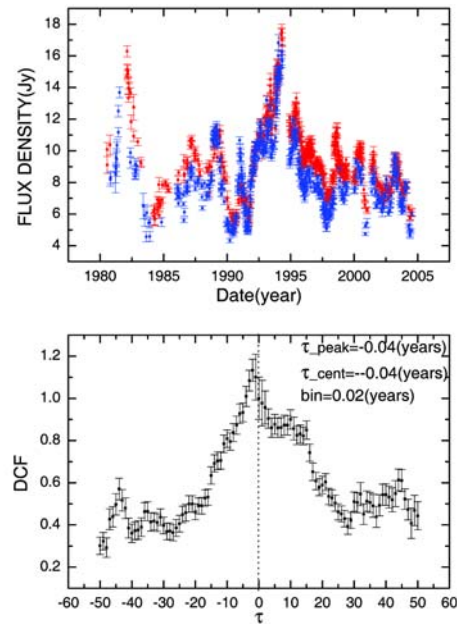


Fig. 4 Top panel shows the light curve of 3C 454.3 at 22 GHz (red dots) and 37 GHz (blue dots), bottom panel the DCF result.

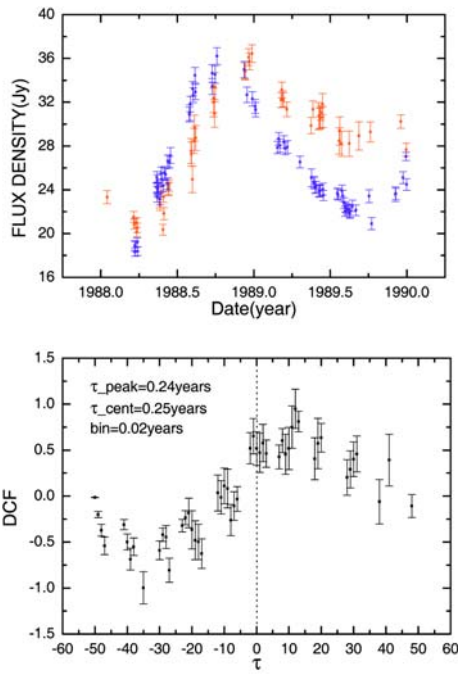


Fig. 5 Top panel shows the light curve of 3C 273 (88–89) at 22 GHz (red dots) and 37 GHz (blue dots), bottom panel the DCF result.

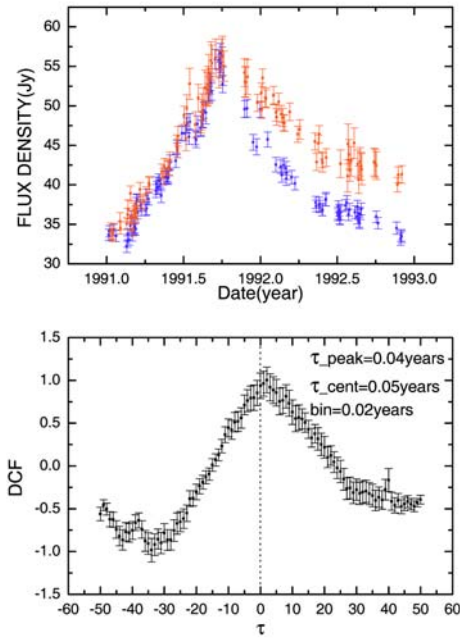


Fig. 6 Top panel shows the light curve of 3C 273 (91–92) at 22 GHz (red dots) and 37 GHz (blue dots), bottom panel the DCF result.

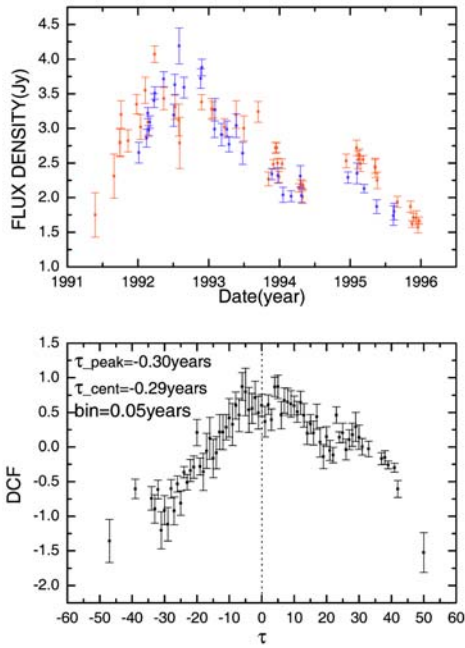


Fig. 7 Top panel shows the light curve of AO 0235+164 at 22 GHz (red dots) and 37 GHz (blue dots), bottom panel the DCF result.

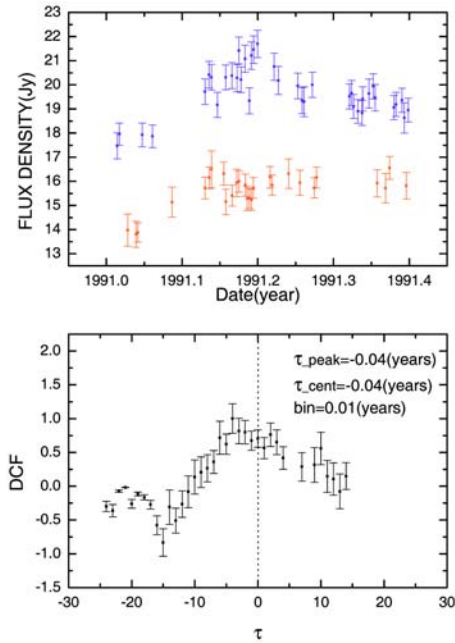


Fig. 8 Top panel shows the light curve of 3C 279 (91) at 22 GHz (red dots) and 37 GHz (blue dots), bottom panel the DCF result.

lag between the two radio bands, except in the data of 91. In the 91's light curve we find a probable lead of the 22 GHz variations leading the 37 GHz ones. The DCF result has a negative peak at 0.04 yr (see Fig. 8), while the ZDCF shows a negative peak at 0.03 yr. The two results are consistent with each other within the uncertainty of ZDCF. The detailed results are in Table 1.

4.3 3C 345

The general shape of the two light curves of this source is strikingly similar, and both light curves are dominated by two strong and long-lasting outbursts. The DCF result shows a positive lag at 0.39 yr, but the ZDCF analysis shows no lag. We also calculated the DCF and ZDCF for the two strong bursts, and the analysis of the 91–92's bursts shows a clear positive lag of 0.12 yr. The DCF and ZDCF results are entirely consistent with each other (see Table 1).

4.4 3C 454.3

This source is a strong radio source and an optically violent variable (OVV) quasar ($z=0.859$). The DCF of all the data shows a negative peak at 0.04 yr, like the previous three sources, while the ZDCF shows no lag. The 90–91 and 94–95 bursts show positive lags near 0.1 yr in both the DCF and ZDCF analyses.

5 DISCUSSION AND CONCLUSIONS

Our main results can be summarized as follows.

- (1) The DCF of each source is close to a gauss profile (Figs.1–8), implying that all the sources have striking correlations between 22 GHz and 37 GHz.
- (2) We find that the 92–96 outburst of AO 0235+164 and the 1991 outburst of 3C 279 both show negative lags, and this is very remarkable because negative lags are rare (Figs. 7 and 8).
- (3) If we use all of the data in the calculation, then we find no clear lags, and the uncertainties are very large. The burst-by-burst analysis shows that different outbursts of some sources have different lags. The analyses of the outbursts of 3C 273 in 88–89 and 96–97, of 3C 279 in 88–89, of 3C 345 in 91–92, and of CTA 102 in 97–98, all show positive lags with 37 GHz leading 22 GHz. Some results of burst-by-burst analysis show no clear lags.
- (4) We find that there is no difference between different sub-class AGNs as regards the time lag between 22 GHz and 37 GHz bursts.

In fact, we would obtain the average result of all the bursts of a source if we use the whole of the data of that source. In previous work, many authors use all the data of one source in the analysis, this is not felicitous and the results are likely to be untrustworthy.

The negative lag is very interesting. In the accelerated jet models, a common assumption is that the particles are accelerated in strong magnetohydrodynamic (MHD) shocks by the Fermi I mechanism (Bell 1978; Blandford & Ostriker 1978). We suggest that, before the particles are accelerated, a major fraction of the particles has very low energies. The energization of the electrons is not only restricted to the shock front, but also in other parts of the jets. When a flare occurs, accelerating mechanism may dominate this process until the radiation reaches a maximum. Then the peak of the energy distribution of particles moves from low to high, resulting in lower frequency leading higher frequency, that is, the negative lag. Marscher (2006) also thought that non-uniform particle acceleration should yield a mixture of time-delayed and simultaneous flares at different frequencies.

The positive lag is well consistent with the shock acceleration mechanism in the jet model. In the jet comoving frame, the typical synchrotron emission frequency of relativistic electrons with γ is

$$\nu_{\text{syn}} = \frac{4}{3}\nu_{\text{B}}\gamma^2, \quad (4)$$

where ν_{B} is Larmor frequency (Bai et al. 2003). It can be seen in Equation (4) that high energy electrons emit synchrotron radiation of high frequencies, and then the electrons cool down to emit in lower frequencies. This process can result in time lag between high and low frequencies. In our work, we assume that the time lag between the peaks (not the beginnings) at high and low frequencies is dominated by the synchrotron

cooling process, and then the light crossing time is unimportant (Zhang et al. 2002; Chiaberge & Ghisellini 1999). In the jet comoving frame, the frequency-dependent time delay is

$$t_{\text{lag}} \approx 2 \times 10^4 [(1+z)/\delta]^{-1/2} B^{-3/2} (\nu_2^{-1/2} - \nu_1^{-1/2}), \quad (5)$$

where z is redshift, B is in units of Gauss, ν in units of 10^{15} Hz in the observer's frame, ν_1 the high frequency, ν_2 the low frequency, and t_{lag} is in units of second. According to Equation (5), we can calculate the magnetic field strength B (assuming the Doppler factor, $\delta = 10$). In the comoving frame of jet, the typical value of B is around $0.01 \sim 0.02$ gauss.

Some bursts show no lag, and a possible explanation of this is that the origin of variations is not intrinsic. The reason for this may be that the jet region is bent, thus the beaming effect is changed, or there are effects of gravitational lensing.

Acknowledgements We are thankful to Metsähovi radio monitoring program for providing the data. This work is supported by the National Natural Science Foundation of China (Grants 10573030 and 10533050) and Natural Science Foundation of Yunnan Province (Grant 2003A0025Q). J. M. B. thanks support of the Bai Ren Ji Hua Project of the CAS.

References

- Alexander T., 1997, In: Maoz D., Sternberg A., Leibowitz E. M. eds., *Astronomical Time Series*, Dordrecht: Kluwer, p.163
- Andrew B. H., Harvey G. A., Medd W. J. et al., 1974, *ApJ*, 191, 51
- Bai J. M., Lee M. G., 2003, *ApJ*, 585, 113
- Balonek T. J., Dent W. A., 1980, *ApJ*, 240, 3
- Balonek T. J., 1982, Ph. D. Thesis, University of Massachusetts
- Bell A. R., 1978, *MNRAS*, 182, 443
- Blandford R. D., Ostriker J. P., 1978, *ApJ*, 221, 29
- Bregman J. N., Glassgold A. E., Huggins P. J. et al., 1988, *ApJ*, 331, 746
- Chiaberge M., Ghisellini G., 1999, *MNRAS*, 306, 551
- Ciprini S., Tosti G., Teräsranta H. et al., 2004, *MNRAS*, 348, 1379
- Clements S. D., Smith A. G., Aller H. D. et al., 1995, *AJ*, 110, 529
- Dent W. A., Balonek T. J., Smith A. G. et al., 1979, *ApJ*, 227, 9
- Edelson R. A., Krolik J. H., 1988, *ApJ*, 333, 646
- Hanski M. T., Takalo L. D., Valtaoja E., 2002, *A&A*, 394, 17
- Hufnagel B. R., Bregman J. N., 1992, *ApJ*, 386, 473
- Kikuchi S., Tabara H., Mikami Y. et al., 1973, *PASJ*, 25, 555
- Kinman T. D., Wardle J. F. C., Conklin E. K. et al., 1974, *AJ*, 79, 349
- Lainela M., 1994, *A&A*, 286, 408
- Marscher A. P., Gear W. K., 1985, *ApJ*, 298, 114
- Marscher A. P., 2006, *Chin. J. Astron. Astrophys. (ChJAA)*, 6S, 262
- Norris J. P., Marani G. F., Bonnell J. T., 2000, *ApJ*, 534, 248
- Peng Z. Y., Lu R. J., Qin Y. P. et al., 2007, *Chin. J. Astron. Astrophys. (ChJAA)*, 7, 428
- Peterson B. M., 2001. In: Itziar Aretxaga, Daniel Kunth, Ral Mjica, eds., *Advanced Lectures on the Starburst-AGN Connection*, Proceedings of a Conference held in Tonantzintla, Puebla, Mexico, 26–30 June, 2000, Singapore: World Scientific, p.3
- Pomphrey R. B., Smith A. G., Leacock R. J. et al., 1976, *AJ*, 81, 489
- Pyatunina T. B., Kudryavtseva N. A., Gabuzda D.C. et al., 2006, *MNRAS*, 373, 1470
- Raiteri C. M., Villata M., Aller H. D. et al., 2001, *A&A*, 377, 396
- Raiteri C. M., Villata M., Tosti G. et al., 2003, *A&A*, 402, 151
- Raiteri C. M., Villata M., Ibrahimov M. A. et al., 2005, *A&A*, 438, 39
- Roy M., Papadakis I. E., Ramoscolón, E. et al., 2000, *ApJ*, 545, 758
- Teräsranta H., Tornikoski M., Valtaoja E. et al., 1992, *A&AS*, 94, 121
- Teräsranta H., Tornikoski M., Mujunen A. et al., 1998, *A&AS*, 132, 305
- Teräsranta H., Achren J., Hanski M. et al., 2004, *A&A*, 427, 769

- Teräsraanta H., Wiren S., Koivisto P. et al., 2005, *A&A*, 440, 409
Tornikoski M., Valtaoja E. Teräsraanta H. et al., 1994a, *A&A*, 286, 80
Tornikoski M., Valtaoja E. Teräsraanta H. et al., 1994b, *A&A*, 289, 673
Türler M., Courvoisier T. J. -L., Paltani S., 2000, *A&A*, 361, 850
Usher P. D., 1972, *ApJ*, 172, 25
Usher P. D., 1975, *ApJ*, 198, 57
Usher P. D., 1979, *AJ*, 84, 1253
Valtaoja E., Teräsraanta H., Urpo S. et al., 1992, *A&A*, 254, 71
Valtaoja L., Sillanpää A., Valtaoja E., 1987, *A&A*, 184, 57
Véron-Cetty M. P., & Véron P., 2006, *A&A*, 455, 773
Villata M., Raiteri C. M., Aller M. F. et al., 2007, *A&A*, 464, 5
Xie G. Z., Li K. H., Zhang Y. H. et al., 1994, *A&AS*, 106, 361
Yi T., Liang E., Qin Y. et al., 2006, *MNRAS*, 367, 1751
Yi T. F., Xie G. Z., 2008, *PASJ*, 60, in press, arXiv: 0803.3409
Yi T. F., Xie G. Z., Zhang F. W., 2008, *Chin. J. Astron. Astrophys. (ChJAA)*, 8, 81
Zhang F. W., Qin Y. P., Zhang B. B., 2007, *PASJ*, 59, 857
Zhang Y. H., Treves A., Celotti A. et al., 2002, *ApJ*, 572, 762